

# Cosmic string formation by flux trapping

Jose J. Blanco-Pillado, Ken D. Olum, and Alexander Vilenkin

*Institute of Cosmology, Department of Physics and Astronomy,  
Tufts University, Medford, MA 02155, USA*

## Abstract

We study the formation of cosmic strings by confining a stochastic magnetic field into flux tubes in a numerical simulation. We use overdamped evolution in a potential that is minimized when the flux through each face in the simulation lattice is a multiple of the fundamental flux quantum. When the typical number of flux quanta through a correlation-length-sized region is initially about 1, we find a string network similar to that generated by the Kibble-Zurek mechanism. With larger initial flux, the loop distribution and the Brownian shape of the infinite strings remain unchanged, but the fraction of length in infinite strings is increased. A 2D slice of the network exhibits bundles of strings pointing in the same direction, as in earlier 2D simulations. We find, however, that strings belonging to the same bundle do not stay together in 3D for much longer than the correlation length. As the initial flux per correlation length is decreased, there is a point at which infinite strings disappear, as in the Hagedorn transition.

## I. INTRODUCTION

Formation of linear defects (strings) at a symmetry-breaking phase transition is of great interest both in cosmology and in condensed matter physics. For a global symmetry breaking, defects are formed because the phases of the Higgs field (order parameter) are uncorrelated on scales greater than the characteristic correlation length  $\xi_H$ . In the simplest case of a global  $U(1)$  symmetry, a string is formed whenever the phase changes by  $2\pi$  around a closed loop. This is the familiar Kibble-Zurek mechanism [1, 2]. The statistical properties of the resulting string networks have been studied in numerical simulations [3], with the following conclusions.

The string network consists of two components: infinite strings and closed loops. The infinite strings constitute about 80% of the total string length and have the shape of random walks; their fractal dimension is  $D = 2$ , within statistical errors. The number of closed loops of length between  $l$  and  $l + dl$  per unit volume is given by

$$n(l)dl = A\xi_H^{-3/2}l^{-5/2}dl, \quad (1)$$

where  $A \sim 1$  is a numerical coefficient. Long Brownian loops of length  $l$  have size  $R \sim (\xi_H l)^{1/2}$ , and Eq. (1) gives a scale-invariant size distribution,

$$n(R)dR \sim R^{-4}dR. \quad (2)$$

Later work showed that these properties are very robust. In particular, simulations of  $Z_2$ -string formation, which require a different symmetry breaking scheme, yield very similar results, except the fraction of length in closed loops is reduced from  $\sim 20\%$  to  $\sim 6\%$  [4, 5].

In the case of a gauge symmetry breaking, each string carries a quantum of magnetic gauge flux, and apart from the Kibble-Zurek mechanism, an additional mechanism of string formation can operate [6]. Any magnetic gauge field present before the phase transition will tend to be squeezed into quantized flux tubes after the phase transition. This mechanism may operate in superconductors, where the stochastic magnetic field can be produced by thermal fluctuations, and in cosmological phase transitions, where the field can be due either to thermal or to quantum fluctuations. Flux trapping becomes the dominant mechanism of string formation when the magnetic field fluctuations get sufficiently large, so that the typical area over which the magnetic flux is equal to one flux quantum is smaller than  $\xi_H^2$  [6]. This condition is often satisfied in superconductors and may well be satisfied in a cosmological setting.

Another interesting example where flux trapping may be important is the brane inflation model. Inflation in this model is driven by the attractive interaction energy of a  $D3$  and an anti- $D3$  brane separated in extra dimensions [7]. The branes eventually collide and annihilate, and cosmic  $D$ -strings ( $D1$ -branes) can be produced in the process [8, 9, 10, 11]. It has been argued in [10] that  $D$ -string formation by Kibble-Zurek mechanism is strongly suppressed in this model. However, a string network may still be formed by flux trapping. Quantum fluctuations of the gauge fields living on the branes get strongly amplified in the process of brane annihilation [12]. The resulting magnetic fields can then be squeezed into quantized flux tubes to become  $D$ -strings. Fundamental ( $F$ ) strings can be formed in a similar manner, by squeezing the electric component of another gauge field (orthogonal to that responsible for  $D$ -strings) into electric flux tubes.<sup>1</sup>

---

<sup>1</sup> If both  $F$  and  $D$  strings are present, they can form bound states and combine into an  $FD$  network [10, 11].

String networks formed by flux trapping may be rather different from those formed by the Kibble-Zurek mechanism. An important parameter here is the rms magnetic flux  $\Phi_c$  through an area  $\xi_B^2$ , where  $\xi_B$  is the correlation length of the magnetic field. If  $\Phi_c$  is much greater than one flux quantum, then the strings will form in bundles containing many strings each [6, 13, 14, 15]. This phenomenon has been observed in 2-dimensional simulations, where vortices (and anti-vortices) had a tendency to bundle together for large values of  $\Phi_c$ . However, the properties of 3-dimensional string networks formed by flux trapping remain largely unknown. What are the shapes of long strings? Are they still Brownian? What fraction of the total length is in closed loops and what is their size distribution? If long strings form bundles, do they tend to stay in the same bundle, or switch from one bundle to another? To address these questions, we have developed a numerical simulation of string formation by flux trapping.

Simulations of detailed Higgs and gauge field dynamics in a phase transition are computationally expensive, and the maximum simulation size that we could achieve in this way would not be sufficient to get a good handle on the statistical properties of string networks. We therefore took a different approach. Our starting point is a stochastic magnetic field, which has presumably originated from either thermal or quantum fluctuations. We put the field on a lattice and use a relaxation technique to relax it to a state in which the flux through each plaquette is an integer multiple of the flux quantum. Strings can then be easily traced by following the flux lines from one cell to another. The net flux into each lattice cell remains equal to zero throughout the relaxation process, ensuring the continuity of strings. A “practical” application of these simulations is that they can be used as initial conditions for dynamical simulations of evolving string networks.

## II. SIMULATION

### A. Initial Conditions

We have performed a series of numerical simulations borrowing techniques previously used in lattice field theory (see for example Ref. [16]). We set up an initial configuration for the magnetic field on a cubic lattice by assigning the values of the vector field  $\mathbf{A}(\mathbf{x})$  to the lattice links. It is then straightforward to compute the magnetic field flux through an individual plaquette from the values of the vector field on its boundaries. Since we are only interested in the magnetic part of the gauge field, it is sufficient to consider a vector potential of the form

$$\mathbf{A}(\mathbf{x}) = \sum_{\mathbf{k}} (2V\omega_{\mathbf{k}})^{-1/2} \mathbf{a}(\mathbf{k}) e^{i\mathbf{k}\cdot\mathbf{x}}, \quad (3)$$

where  $\omega_{\mathbf{k}} = |\mathbf{k}|$ ,  $V = L^3$  is the volume of the simulation box, and we use the system of units in which  $\hbar = c = 1$ . The reality of the electromagnetic field is ensured by the constraint,  $\mathbf{a}(-\mathbf{k}) = \mathbf{a}^*(\mathbf{k})$ .

We impose periodic boundary conditions, so the wave vector  $\mathbf{k}$  takes a discrete set of values,  $\mathbf{k} = (2\pi/L)\mathbf{n} = (2\pi/L)(n_1, n_2, n_3)$  with  $n_1, n_2, n_3 = 0, \pm 1, \dots$ . The number of lattice points along each side of the box is  $N = L/\Delta x$ , where  $\Delta x$  is the lattice spacing. Wavelengths shorter than  $2\Delta x$  cannot be represented in such a lattice, so we cut off the summation in (3) at  $n_j = \pm N/2$ ,

$$\mathbf{A}(\mathbf{x}_{\mathbf{m}}) = \sum_{\mathbf{n}} (4\pi L^2 |\mathbf{n}|)^{-1/2} \mathbf{a}(\mathbf{n}) e^{2\pi i \mathbf{n} \cdot \mathbf{m} / N}. \quad (4)$$

Here, we have denoted the points on the lattice by  $\mathbf{x}_{\mathbf{m}} = \Delta x \mathbf{m} = \Delta x (m_1, m_2, m_3)$ .

We obtain particular realizations of the vector field by drawing the values of the coefficients  $\mathbf{a}(\mathbf{k})$  from an appropriate Gaussian distribution. In the case of superconductors, the distribution is expected to have a thermal (Rayleigh-Jeans) form, with a cutoff at short wavelengths [15],

$$\langle a_i^*(\mathbf{k}) a_j(\mathbf{k}') \rangle = \frac{K}{\omega_{\mathbf{k}}} e^{-(k/k_c)^2} \delta_{ij} \delta_{\mathbf{k}\mathbf{k}'}, \quad (5)$$

where  $k_c$  is related to the dissipation rate of the magnetic field, and  $K$  gives the amplitude of the spectrum, which in the thermal case is just the temperature. Defining the cutoff wavelength  $\lambda_c = 2\pi/k_c$ , we can rewrite this as

$$\langle a_i^*(\mathbf{n}) a_j(\mathbf{n}') \rangle = \frac{KL}{2\pi |\mathbf{n}|} e^{-(\lambda_c |\mathbf{n}| / L)^2} \delta_{ij} \delta_{\mathbf{n}\mathbf{n}'}. \quad (6)$$

This form of the spectrum for gauge field fluctuations has also been found in brane inflation models, with  $k_c \sim K \sim 1/\tau$ , where  $\tau$  is the characteristic timescale of brane annihilation [12].

## B. Relaxation technique

Once the initial conditions for the magnetic field have been set, we need a mechanism that confines the field into strings carrying a fundamental unit of flux,

$$\Phi_0 = e^{-1} \equiv \alpha^{-1/2}, \quad (7)$$

where  $e$  is the gauge coupling. Our final state should then have the magnetic flux through all plaquettes equal either to zero or to an integral multiple of  $\Phi_0$ . This will allow us to follow the flux around the simulation box to find the corresponding network of strings.

In Appendix A, we compute the the rms magnetic flux  $\Phi_c$  through a disk of diameter  $\lambda_c$  in the spectrum of Eq. (6). We define the rms number of flux quanta in such a disk,

$$\mathcal{N} = \Phi_c / \Phi_0 \approx 0.46 (K \alpha \lambda_c)^{1/2}. \quad (8)$$

For  $\mathcal{N} > 1$ , strings are expected to form bundles with several strings per bundle. The typical number of strings in a bundle is larger than  $\mathcal{N}$ , because bundles appear not in random places but where the flux in a given direction is larger than usual.

As mentioned before, the vector field  $\mathbf{A}$  lives naturally on the links of the lattice and enters the computation of the magnetic flux through the adjacent plaquettes. It is clear that changing the value of the gauge field on a link separating two plaquettes will only displace part of the flux from one of those plaquettes to the other, keeping the total flux unchanged. We would like to implement an algorithm that will drive the magnetic flux through each plaquette to one of the values  $\Phi = n\Phi_0$  with  $n = 0, \pm 1, \dots$ . We accomplish this by evolving the vector field  $A_l$  on each link  $l$  according to the following equation of motion,

$$\frac{dA_l}{dt} = - \sum_{l \in f} \frac{\partial V(\Phi_f)}{\partial A_l}, \quad (9)$$

where the sum is performed over all four plaquettes that have  $l$  as a side and  $V(\Phi_f)$  is a function of the magnetic flux  $\Phi_f$  through the  $f$ -th plaquette that has its minima at  $\Phi = n\Phi_0$ . (It is assumed that  $V(-\Phi) = V(\Phi)$ , so  $V(\Phi)$  is independent of how one chooses the direction normal to the plaquette.) Eq. (9) describes an overdamped system which is driven to the minimum of the potential energy,

$$U = \sum_f V(\Phi_f), \quad (10)$$

where the summation is taken over all the plaquettes in the lattice. The form of the function  $V(\Phi)$  that we used in the simulation is given in Appendix B. This particular form is not essential for the method to work, although it is important to make sure that the final flux through a plaquette is approached in a smooth and monotonic way. This is achieved by choosing the time step  $\Delta t$  of the simulation sufficiently small.

We finally have to choose a suitable lattice spacing  $\Delta x$ . A natural choice is to set it equal to the correlation length,  $\Delta x = \lambda_c$ , as it was done in earlier simulations of string formation by the Kibble mechanism [3, 4, 5]. This works fine when the parameter  $\mathcal{N} = \Phi_c/\Phi_0 \lesssim 1$ , but for large values of  $\mathcal{N}$  there is a large number of strings per lattice cell, which makes it hard to resolve individual strings. Hence, we used

$$\Delta x \sim \begin{cases} \lambda_c & \mathcal{N} \leq 1 \\ \lambda_c \mathcal{N}^{-1/2} & \mathcal{N} > 1. \end{cases} \quad (11)$$

The overdamped evolution of Eq. (9) converges on a state where the “potential energy” of Eq. (10) vanishes because the flux is properly quantized. However, this evolution may be quite slow, because some plaquettes may have flux nearly equidistant between two multiples of  $\Phi_0$  and so have little force driving them toward one or another.

At a phase transition that confines flux into strings, a loop of flux can also shrink down to nothing. (For example, if there is a loop with less than half a quantum of flux, this must happen.) In general, in a region with no net flux to the outside (as we have because of periodic boundary conditions), in a slow phase transition the flux will tend to diffuse to nothing, whereas in a rapid transition it will tend to be quantized. In the simulation, this choice is affected by the size of  $\Delta x$ . If  $\Delta x$  is taken so small that the average number of flux quanta through each plaquette is much less than 1, then the algorithm takes a long time to assemble a whole quantum of flux, and the flux tends to dissipate, so that there are very few strings. Thus even if  $\mathcal{N}$  is large, if we make  $\Delta x$  small we get primarily dissipation. Since we are interested in studying the shape of the string network, we will not make this choice. However, when  $\mathcal{N}$  is small, even if we choose  $\Delta x \sim \lambda_c$  as in Eq. (11), the average flux per plaquette will still be small, and so the diffusion of the flux may become important.

### III. RESULTS

#### A. Large $\mathcal{N}$

We are mainly interested in studying the properties of a string network with a reasonably large number of strings per bundle. We have generated initial conditions for this type of configuration by setting  $\lambda_c = 6\Delta x$  and  $\mathcal{N} \sim 3.2$ . The result of the relaxation procedure

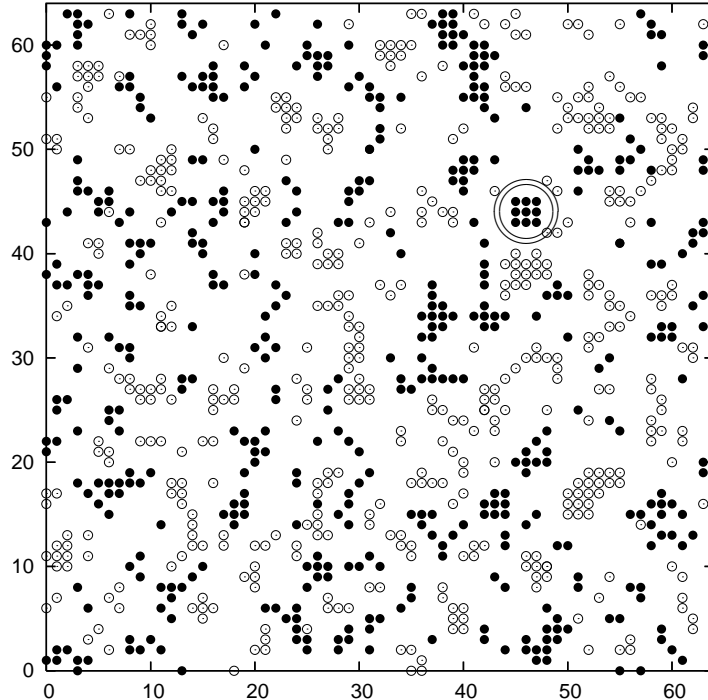


FIG. 1: Two-dimensional slice of a  $64^3$  lattice simulation. The black and white circles represent the position of vortices and anti-vortices respectively. Clusters of vortices (anti-vortices) are clearly visible in this figure, indicating that the corresponding strings in the 3D lattice form bundles that pierce this surface with the same orientation. We encircled the particular group of vortices that we study in detail in Fig. 2.

shows that a typical 2D slice of the final configuration has several bunches, some of them including 10 strings or more. We show in Fig. 1 a 2D slice of a  $64^3$  lattice simulation. As one might expect, it resembles the 2D simulations discussed in Refs. [13, 14].

To find out how long the string bunches stay together, we followed the three-dimensional trajectories of strings for a few steps in both directions, starting from the bunch encircled in Fig. 1. The result is plotted in Fig. 2. We see that the strings only stay together for a few steps, quickly branching off in different directions (and possibly joining other bunches).

We have also computed the fractal dimension of strings by averaging the distance  $R$  between points separated by length  $l$  along the string. We have computed this function  $R(l)$  by averaging over all sufficiently long strings present in 30 realizations; the result is shown in Fig. 3.

The best fit to the data is given by

$$R = Al^\beta, \quad (12)$$

with

$$A = 2.00 \pm 0.05 \quad \beta = 0.52 \pm 0.01, \quad (13)$$

where all lengths are measured in units of  $\Delta x$ . The stated errors here and below are an indication of the uncertainty in the parameter values, based on differences between separate runs. Equation (12) is consistent with a random walk shape,  $\beta = 1/2$ , of the strings at large

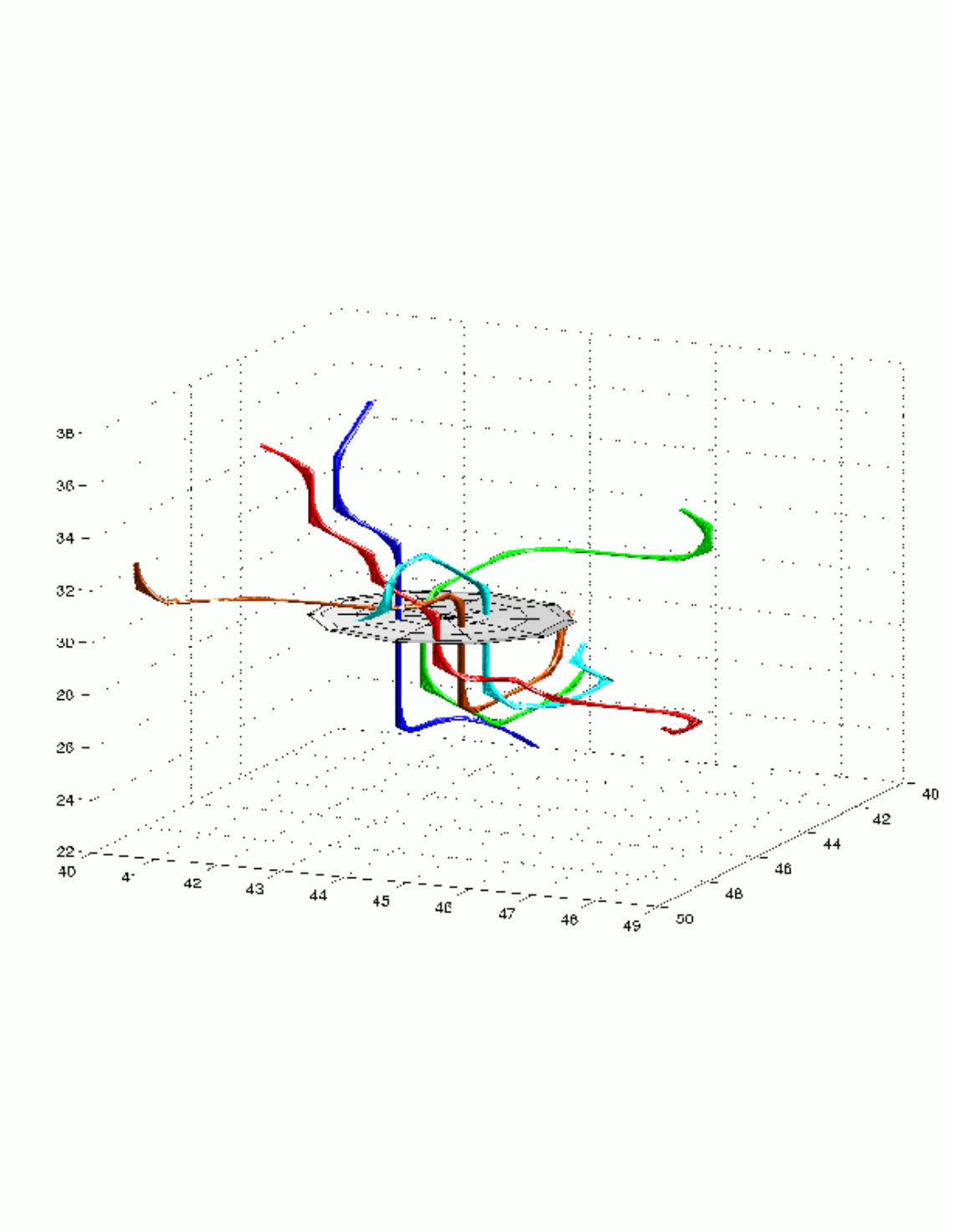


FIG. 2: 3D structure of 5 of the 9 strings encircled in Fig. 1. We also plot a small portion of the 2D slice to indicate the region of space where the strings come together as they go through that plane.

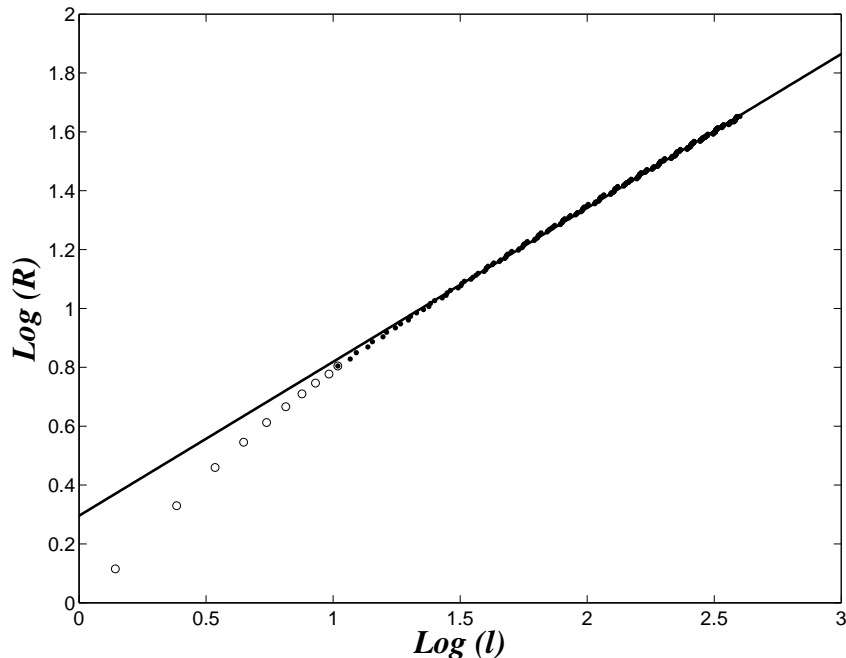


FIG. 3: Average displacement between two points on the string versus the corresponding length along the string for the case with  $\mathcal{N} \sim 3.2$ . Here and below white circles indicate points which are not included in the numerical fit.

$R$ . The effective step of the random walk,  $\xi \sim A^2 \sim 4$ , is comparable to  $\lambda_c$ , as expected. It is also comparable to the characteristic length for which strings in a bundle stay together.

Since our simulations were performed in a box with periodic boundary conditions, all the strings found in the lattice are, in fact, closed loops. The infinite string component of the network is represented by very long strings, which wind many times around the box. We counted all strings shorter than  $2L$  as loops and the rest as infinite strings, but our results are insensitive to the particular choice of  $2L$  as the separation between these two components of the network. We found that the fraction of energy stored in infinite strings is about 98% versus 2% in closed loops.

The length distribution of loops is shown in Fig. 4. The best fit to the data for sufficiently large loop sizes is

$$n(l)dl = Bl^{-\gamma}dl, \quad (14)$$

with the following parameters,

$$B = 0.017 \pm 0.001 \quad \gamma = 2.50 \pm 0.03 \quad (15)$$

Once again, this is consistent with the scale-invariant distribution of Eqs. (1,2).

## B. $\mathcal{N} \sim 1$

To simulate a network with  $\mathcal{N} \sim 1$ , we have chosen the following parameters:  $\lambda_c = \Delta x$ ,  $\mathcal{N} \sim 0.28$ . These values have been selected to adjust the rms magnetic flux through a

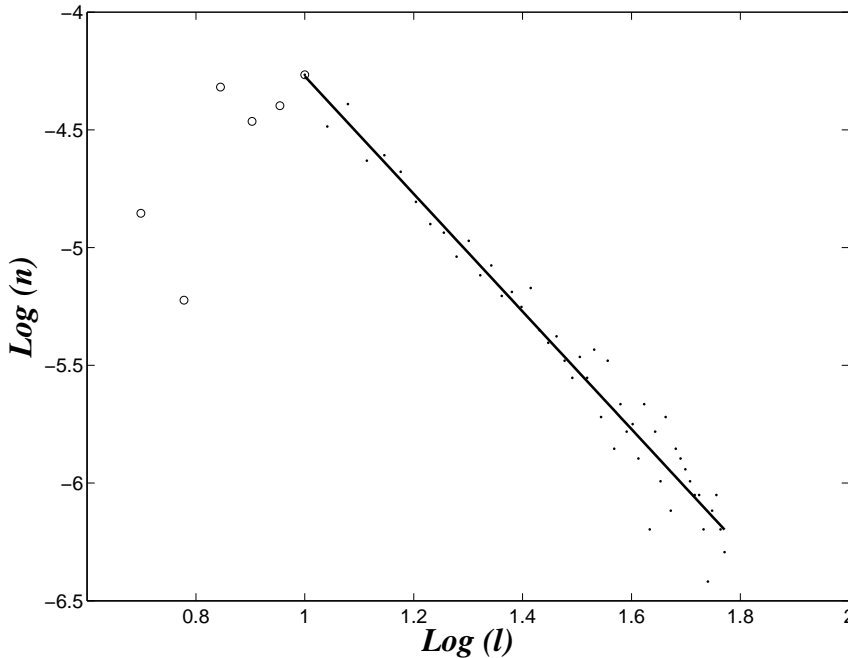


FIG. 4: Spectrum of closed string loops as a function of their length for the case with  $\mathcal{N} \sim 3.2$ .

plaquette to  $0.3\Phi_0$ . This roughly corresponds to the probability of  $\sim 30\%$  of having a string through a plaquette in Kibble mechanism simulations of [3]. With this set of parameters, the magnetic fluxes through neighboring plaquettes are only weakly correlated with one another, so we expect that strings will not form bundles and that the resulting network will be similar to the ones obtained in [3]. And indeed, the results we obtained are nearly identical to those of [3], even though the numerical methods used in the two simulations are rather different in nature.

We have performed these simulations in cubic lattices of size  $16^3$ ,  $32^3$  and  $64^3$  and found that the average fraction of string length in long (infinite) strings was respectively 86%, 84% and 82%. These values are very close to those found in Ref. [3].

The distance versus length along the string,  $R(l)$ , and the length distribution of loops,  $n(l)$ , are plotted in Figs. 5 and 6, respectively, for that largest box of size  $64^3$ . The data are well fitted by Eqs. (12),(14) with

$$A = 1.45 \pm 0.03 \quad \beta = 0.51 \pm 0.01, \quad (16)$$

$$B = 0.065 \pm 0.003 \quad \gamma = 2.51 \pm 0.02. \quad (17)$$

As before, the strings have Brownian shapes and the loops exhibit a scale-invariant distribution.

### C. Small $\mathcal{N}$

To explore the properties of the network for  $\mathcal{N} \ll 1$ , we kept  $\lambda_c = \Delta x$  and gradually decreased  $\mathcal{N}$ , starting from the value of 0.28 cited in the preceding subsection. For  $\mathcal{N} \ll 1$ ,

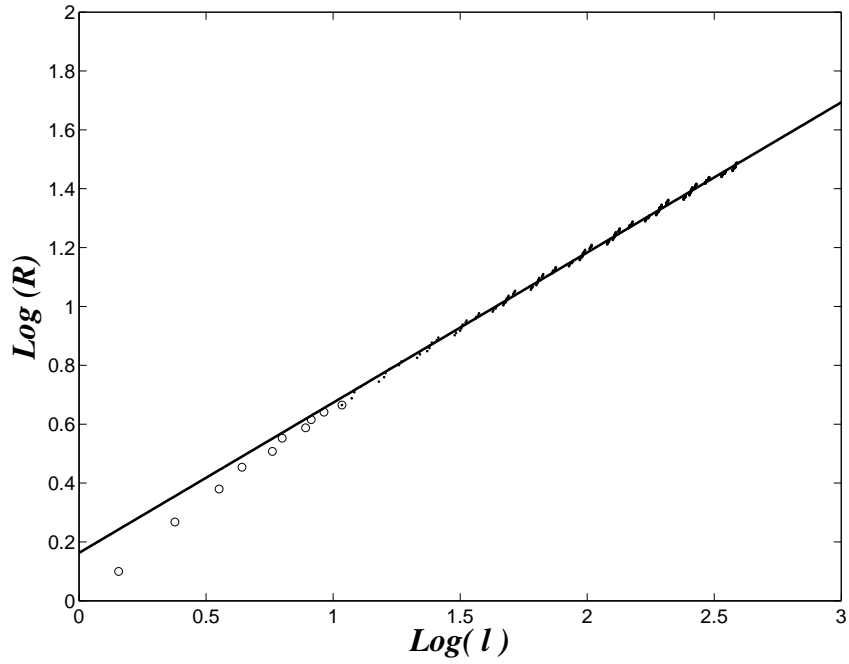


FIG. 5: Average displacement between two points on the string versus the corresponding length along the string for the case with  $\mathcal{N} \sim 0.28$ .

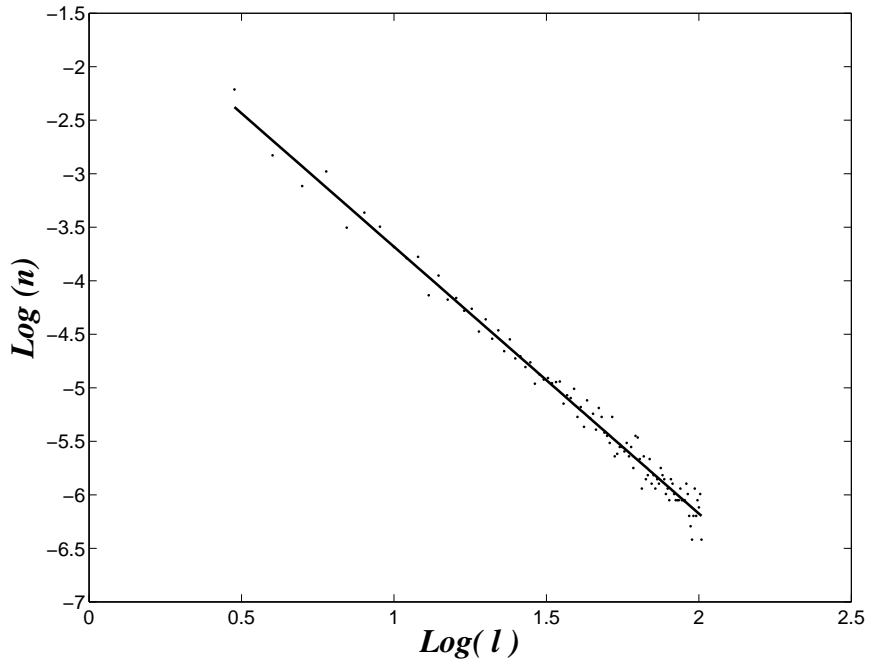


FIG. 6: Spectrum of closed string loops as a function of their length for the case with  $\mathcal{N} \sim 0.28$ .

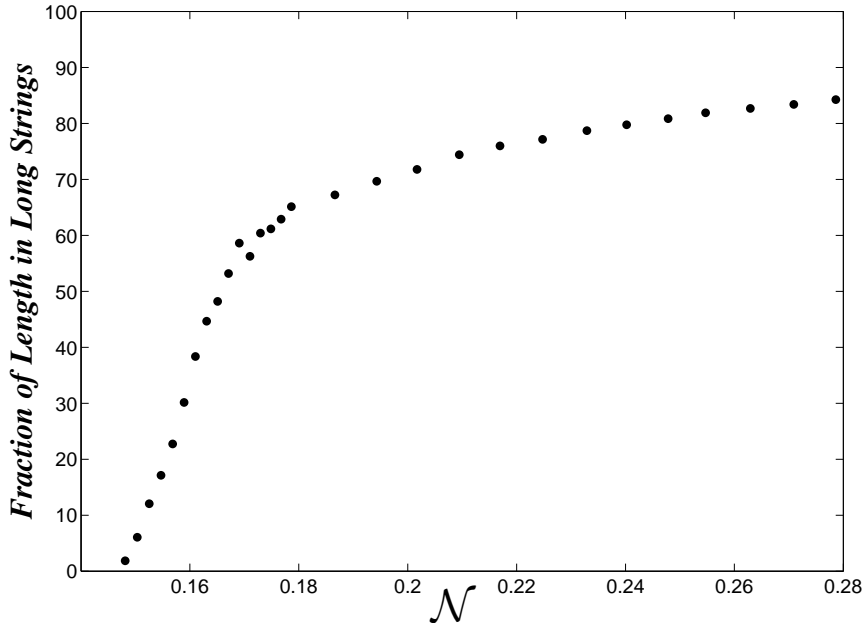


FIG. 7: Fraction of the total string length in infinite strings as a function of the parameter  $\mathcal{N}$ .

the rms flux through a plaquette is much smaller than  $\Phi_0$ . As a result, most plaquettes have no strings. The strings have the form of small closed loops and appear in rare places where the magnetic field fluctuates well above its rms value.

In Fig. 7 we plot the fraction of length in infinite strings as a function of  $\mathcal{N}$ . The simulations discussed in subsections III.A and III.B above correspond to  $\mathcal{N} = 3.2$  and  $\mathcal{N} = 0.28$ , respectively. As  $\mathcal{N}$  is decreased, infinite strings constitute a smaller and smaller fraction of the total string length and finally disappear at  $\mathcal{N}_c \approx 0.15$ . The total string energy density also decreases with the decrease of  $\mathcal{N}$  (see Fig. 8), but remains finite at (and below) the critical value  $\mathcal{N}_c$ . For all values of  $\mathcal{N} > \mathcal{N}_c$  the loop distribution retains its scale-invariant form (1). For  $\mathcal{N} < \mathcal{N}_c$ , most of the string length is in the smallest loops, and the number density of loops  $n(l)$  decreases rapidly with the loop's length  $l$ .

It is interesting to note that very similar behavior is observed in a thermal ensemble of strings with a lower cutoff on the loop length,  $l_{min}$ . As the string length per unit volume is decreased below a certain critical value,  $\rho_c \sim l_{min}^{-2}$ , the system undergoes the Hagedorn transition, characterized by the disappearance of infinite strings. It was noted earlier [17, 18] that string configurations resulting from simulations of Kibble-Zurek-type phase transitions resemble those obtained from a thermal string ensemble.

However, we also note that in this regime, the average flux per plaquette is quite small. This appears to increase the effects of diffusion of the flux as compared to confinement, and so it is possible that the decrease in long strings is due to the increased diffusion.

#### IV. CONCLUSIONS

We have studied the statistical properties of string networks formed by the flux trapping mechanism. As anticipated in earlier analyses [6, 13, 14, 15], the character of the network de-

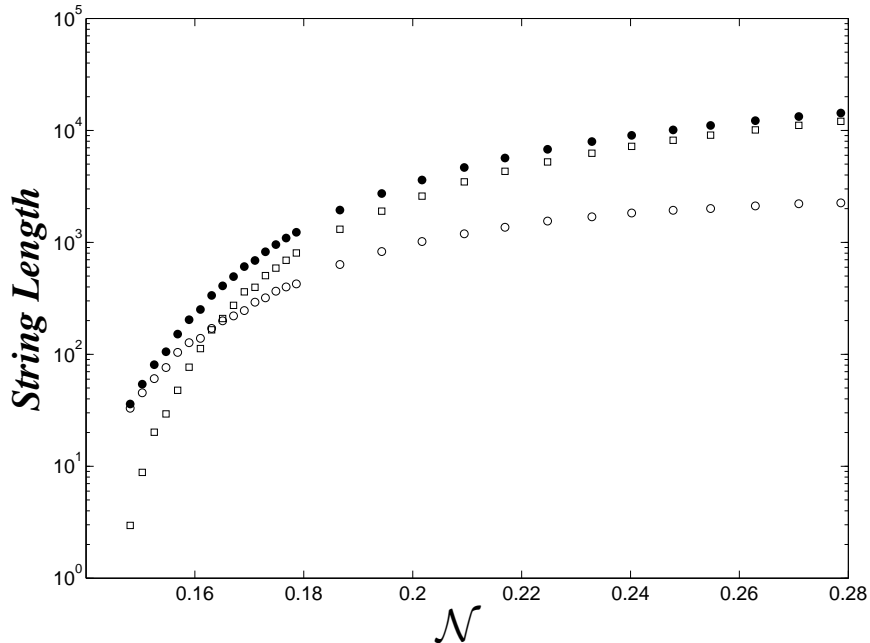


FIG. 8: Plot of the average total string length (black circles) as well as the different contributions from infinite (squares) and closed strings (white circles) as a function of  $\mathcal{N}$ . The average is performed over 100 simulations of a  $32^3$  lattice.

depends on the rms flux through a correlation-size region,  $\Phi_c$ , or equivalently on the parameter  $\mathcal{N} = \Phi_c/\Phi_0$ , where  $\Phi_0$  is the flux quantum.

We found that for large values of  $\mathcal{N}$  most of the string length is in a tangled network of infinite strings, having the shape of random walks, with closed loops contributing only a small fraction of the total length. The step of the random walk is comparable to the correlation length  $\lambda_c$  of the magnetic field. The typical inter-string separation,  $d \sim \lambda_c/\sqrt{\mathcal{N}}$ , can be much smaller. A 2D slice of the simulation exhibits bundles of strings pointing in the same direction, with  $\sim \mathcal{N}$  strings per bundle. We found, however, that strings belonging to the same bundle do not stay together for long. As we follow them in 3D, they part each other's company on a length scale not much exceeding  $\lambda_c$ .

For  $\mathcal{N} \sim 1$ , there are no string bundles, and the properties of the string network are nearly identical to those of the networks formed by the Kibble-Zurek mechanism.

For small values of  $\mathcal{N}$ , the string density is exponentially suppressed and most of the string length is in the form of small loops of length  $l \sim \lambda_c$ .

How does the initial string configuration affect the subsequent evolution of the network? For  $\mathcal{N} \gg 1$ , the properties of the network differ from the standard initial configuration of Ref. [3] on relatively short length scales,  $\mathcal{N}^{-1/2}\lambda_c \lesssim l \lesssim \lambda_c$ , which can have an effect on early string evolution. These effects can be studied by dynamical string simulations in an expanding universe, with initial conditions generated by simulations of the type described here. At late times, the string bundles break apart, and we expect the network evolution to follow the standard scenario (see, e.g., [19]). For type-I strings, which can have arbitrary large winding numbers, the initial configuration with  $\mathcal{N} \gg 1$  may facilitate the formation of higher-winding strings. This may have an effect on the subsequent evolution of the network.

For  $\mathcal{N} \sim 1$ , the initial configuration is similar to the standard one, so the standard evolution scenario is followed from the very beginning. Finally, for  $\mathcal{N} \ll 1$ , all strings are in the form of small closed loops, which rapidly shrink and disintegrate.

## ACKNOWLEDGMENTS

This work was supported in part by the National Science Foundation under grants 0457456 and 0353314.

## APPENDIX A: AVERAGE FLUX THROUGH A DISK

We want to compute the rms magnetic flux through a disc of radius  $R$ . We follow similar calculations done in [14, 15]. The mean square flux is

$$\langle \Phi(R)^2 \rangle = \left\langle \int_0^R d^2x d^2y B_z(x, z=0) B_z(y, z=0) \right\rangle. \quad (\text{A1})$$

Using our definition for  $\mathbf{A}$  given in Eq. (3), this becomes

$$\langle \Phi(R)^2 \rangle = \int_0^R d^2x d^2y \sum_{\mathbf{q}, \mathbf{k}} (4V^2 \omega_{\mathbf{q}} \omega_{\mathbf{k}})^{(-1/2)} [q_x k_x \langle a_y^*(\mathbf{q}) a_y(\mathbf{k}) \rangle + q_y k_y \langle a_x^*(\mathbf{q}) a_x(\mathbf{k}) \rangle] e^{i(\mathbf{k} \cdot \mathbf{x} - \mathbf{q} \cdot \mathbf{y})}.$$

By  $\mathbf{x}$  and  $\mathbf{y}$  we mean the 3-vectors whose  $z$  component is 0, and we have neglected the cross terms that average to zero. Using now equation (5) we arrive at

$$\langle \Phi(R)^2 \rangle = \int_0^R d^2x d^2y \sum_{\mathbf{k}} (2V \omega_{\mathbf{k}})^{-1} (k_x^2 + k_y^2) \frac{K}{\omega_{\mathbf{k}}} e^{-(k/k_c)^2} e^{i\mathbf{k} \cdot (\mathbf{x} - \mathbf{y})}, \quad (\text{A2})$$

where  $k$  is the length of  $\mathbf{k}$ . We now take the infinite volume limit and replace the sum by an integral, using

$$\frac{1}{V} \sum_{\mathbf{k}} \rightarrow \frac{1}{(2\pi)^3} \int d^3k, \quad (\text{A3})$$

so we can rewrite the expression above in the following form,

$$\langle \Phi(R)^2 \rangle = \frac{K}{2(2\pi)^3} \int_0^R d^2x d^2y \int d^3k \frac{k_{\perp}^2}{k^2} e^{-(k/k_c)^2} e^{i\mathbf{k} \cdot (\mathbf{x} - \mathbf{y})}, \quad (\text{A4})$$

where we have defined  $k_{\perp} = (k_x^2 + k_y^2)^{1/2}$ . We can exchange the order of the integrals to get,

$$\begin{aligned} \langle \Phi(R)^2 \rangle &= \frac{K}{2(2\pi)^3} \int d^3k \frac{k_{\perp}^2}{k^2} e^{-(k/k_c)^2} \left( \int_0^R r dr \int_0^{2\pi} d\theta e^{ik_{\perp} r \cos \theta} \right)^2 \\ &= \frac{K}{4\pi} \int d^3k \frac{k_{\perp}^2}{k^2} e^{-(k/k_c)^2} \left( \int_0^R r dr J_0(k_{\perp} r) \right)^2. \end{aligned}$$

Performing the integral in  $r$  we obtain

$$\langle \Phi(R)^2 \rangle = \frac{KR^2}{4\pi} \int \frac{d^3k}{k^2} e^{-(k/k_c)^2} J_1(k_\perp R)^2 \quad (\text{A5})$$

We now break up the integral into an integral in  $k_z$ , a radial integral in  $k_\perp$ , and a trivial angular integral, to get

$$\begin{aligned} \langle \Phi(R)^2 \rangle &= \frac{KR^2}{2} \int_0^\infty dk_\perp k_\perp J_1(k_\perp R)^2 e^{-(k/k_c)^2} \int dk_z \frac{e^{-(k_z/k_c)^2}}{k_z^2 + k_\perp^2} \\ &= \frac{\pi KR^2}{2} \int_0^\infty dk_\perp J_1(k_\perp R)^2 \operatorname{erfc}(k/k_c) = \frac{\pi KR}{2} \mathcal{F}\left(\frac{\lambda_c}{R}\right), \end{aligned}$$

where

$$\mathcal{F}(z) = \int_0^\infty dy J_1(y)^2 \operatorname{erfc}\left(\frac{yz}{2\pi}\right) = \frac{2\pi^{5/2}}{3z^3} {}_2F_2\left(\frac{3}{2}, \frac{3}{2}, \frac{5}{2}, 3, -\frac{4\pi^2}{z^2}\right) \quad (\text{A6})$$

where  ${}_2F_2$  is a hypergeometric function.

We can now define  $\mathcal{N}$  as the rms flux through a disk of diameter  $\lambda_c$ , i.e.,  $R = \lambda_c/2$ , in fundamental flux units, namely,

$$\mathcal{N} = \frac{\langle \Phi(\lambda_c/2)^2 \rangle^{1/2}}{\alpha^{-1/2}} = (K\alpha\lambda_c)^{1/2} \left(\frac{\pi}{4} \mathcal{F}(2)\right)^{1/2} \approx 0.46(K\alpha\lambda_c)^{1/2} \quad (\text{A7})$$

## APPENDIX B: THE CONFINING POTENTIAL $V(\Phi)$ .

We wish to choose a potential  $V(\Phi)$  which will confine the field by driving the flux through each plaquette to an integer multiple of  $\Phi_0$ . We treat any multiple the same as any other, so  $V$  should be periodic with period  $\Phi_0$ . Similarly, upward and downward flux are to be treated the same, so  $V(\Phi) = V(-\Phi)$ .

We choose an inverted parabola centered at  $\Phi_0/2$ , so that the flux will be driven to the nearest multiple of  $\Phi_0$ . If we continue this parabola all the way to zero, we find that the flux jumps back and forth around zero, instead of settling smoothly to zero. Thus we use a smooth quadratic form for  $V(\Phi)$  near zero. The smoothing extends to a critical value  $\Phi_* = 1/N^2$ . Any larger value can result in one unit flux being spread out throughout the lattice instead of being concentrated on a single plaquette.

Our potential is then given by

$$V(\Phi) = \begin{cases} c_1 \Phi^2 & 0 < \Phi < \Phi_* \\ 1 - c_2 (\Phi_0/2 - \Phi)^2 & \Phi_* < \Phi < \Phi_0/2 \end{cases} \quad (\text{B1})$$

and for other values of  $\Phi$  by reflection and periodicity, with

$$c_1 = \frac{2}{\Phi_* \Phi_0} \quad (\text{B2})$$

$$c_2 = \frac{2}{\Phi_0(\Phi_0/2 - \Phi_*)}, \quad (\text{B3})$$

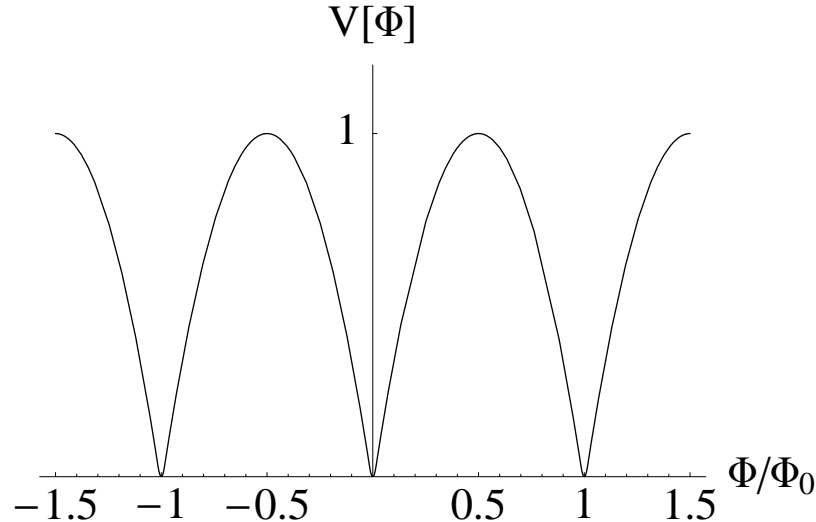


FIG. 9: Confining potential as a function of the magnetic flux through a single plaquette.

which make  $V(\Phi)$  and its derivative continuous at  $\Phi_*$ . We plot in Fig. 9 the potential  $V(\Phi)$  for  $N = 64$ .

We then choose the largest time step  $\Delta t$  which will not allow the potential to overshoot 0 in a single step.

- 
- [1] T.W.B. Kibble, J. Phys. **A9**, 1387 (1976).
  - [2] W.H. Zurek, Nature **317**, 505 (1985).
  - [3] T. Vachaspati and A. Vilenkin, Phys. Rev. **D30**, 2036 (1984).
  - [4] T.W.B. Kibble, Phys. Lett. **166B**, 311 (1986).
  - [5] M. Aryal, A.E. Everett, T. Vachaspati and A. Vilenkin, Phys. Rev. **D34**, 434 (1986).
  - [6] M. Hindmarsh and A. Rajantie, Phys. Rev. Lett. **85**, 4660 (2000).
  - [7] G. Dvali and S.H. Tye, Phys. Lett. **B450**, 72 (1999).
  - [8] S. Sarangi and S.H. Tye, Phys. Lett. **B536**, 185 (2002).
  - [9] N. Jones, H. Stoica and S.H. Tye, JHEP **01**, 036 (2002).
  - [10] G. Dvali and A. Vilenkin, JCAP **0403**, 010 (2004).
  - [11] E.J. Copeland, R.C. Myers and J. Polchinski, JHEP **0406**, 013 (2004).
  - [12] G. Dvali and A. Vilenkin, Phys. Rev. D **67**, 046002 (2003).
  - [13] G.J. Stephens, L.M. Bettencourt and W.H. Zurek, Phys. Rev. Lett. **88**, 137004 (2002).
  - [14] T.W.B. Kibble and A. Rajantie, Phys. Rev. B **68**, 174512 (2003).
  - [15] M. Donaire, T.W.B. Kibble and A. Rajantie, arXiv:cond-mat/0409172.
  - [16] K. D. Olum and J. J. Blanco-Pillado, Phys. Rev. D **60**, 023503 (1999)
  - [17] D. Mitchell and N. Turok, Phys. Rev. Lett. **58**, 1577 (1987); Nucl. Phys. **B294**, 1138 (1987).
  - [18] M. Sakellariadou and A. Vilenkin, Phys. Rev. **D37**, 885 (1988).
  - [19] A. Vilenkin and E.P.S. Shellard, *Cosmic Strings and Other Topological Defects* (Cambridge University Press, Cambridge 2000).